Morphology Transition during Low-Pressure Chemical Vapor Deposition

Y.-P. Zhao, Jason T. Drotar, G.-C. Wang, and T.-M. Lu

Department of Physics, Applied Physics, and Astronomy, Rensselaer Polytechnic Institute, Troy, New York 12180-3590

(Received 28 August 2000; published 10 September 2001)

Assuming a reemission model, we have studied, in detail, the effect of sticking coefficient on the morphology evolution in low-pressure chemical vapor deposition processes. We have shown that the surface morphology changes from a self-affine fractal to a columnarlike morphology with increasing sticking coefficient, which agrees qualitatively with experimental observations.

DOI: 10.1103/PhysRevLett.87.136102 PACS numbers: 68.55.Jk, 05.10.Gg, 64.60.Ht, 81.15.Gh

Recently, by employing the concept of dynamic scaling combined with analytical treatments, including the use of stochastic differential equations and simulations, considerable progress has been made in the basic understanding of growth/etching phenomena [1–3]. In the dynamic scaling hypothesis, the surface is described by the equal-time height-height correlation function $H(\mathbf{r}, t)$, defined as $H(\mathbf{r}) = \langle [h(\mathbf{r}) - h(\mathbf{0})]^2 \rangle$. Here $h(\mathbf{r})$ is the surface height at position $\mathbf{r}$ $[= (x, y)]$ on the surface. The notation $\langle \cdots \rangle$ denotes a statistical average. The scaling hypothesis requires that $H(r) = \rho^2 r^{2\alpha}$ for $r \ll \xi$ and $H(r) = 2w^2$ for $r \gg \xi$ [1–3]. Here ρ is the average local slope, ξ is the lateral correlation length, w is the interface width or RMS roughness, and α is the roughness exponent. Both w and ξ grow as power laws in time, $w \sim t^{\beta}$ and $\xi \sim t^{1/z}$, where the exponents β and z are called growth exponent and dynamic exponent, respectively. One outstanding outcome of the dynamic scaling hypothesis is the existence of universality in which the essential features of roughness evolution, i.e., the α, β, and z values, depend on certain symmetries and the dimensionality of the system, but not on the detailed interactions.

One of the most famous universality classes is the Kardar-Parisi-Zhang (KPZ) roughening model, which was proposed 15 years ago [4]. KPZ-type surface roughening requires that the flux of incoming particles remains spatially constant normal to the surface, so that the growth rate does not vary across the film surface. In other words, the growth must be conformal. In this sense, it is natural for one to expect KPZ-type growth in a chemical vapor deposition (CVD) process, since CVD growth is usually conformal. So far, however, not many CVD experiments have claimed to observe KPZ growth behavior [5]. In fact, CVD is a very complicated process. It includes precursor transport, chemical reaction, and surface interaction. The limiting cases for CVD are the high-pressure and the low-pressure CVD processes. For the high-pressure CVD process, the mean free path of the precursor is much smaller than the characteristic length of the surface features; i.e., the Knudsen number is small (the Knudsen number is defined as the ratio of the mean free path of the precursor to the characteristic length of the surface features). Therefore the CVD process can be described by a hydrodynamic process. For low-pressure CVD (LPCVD), since the mean free path of the precursor is much larger than the characteristic length of the surface features, the CVD process can be described by ballistic transport.

Several researchers have studied surface morphology for the small Knudsen number case [6,7]. Particularly, Bales *et al.* have shown theoretically that, in the diffusion-limited growth regime, the surface is not stable and has a fingerlike morphology [6]. In the reaction-limited growth regime, the surface should, theoretically, exhibit a KPZ type of growth [6], but so far there is not experimental evidence to support this claim. This could be due to complications caused by flow transport. In the large Knudsen number case, the precursor transport is ballistic, and one does not need to worry about the flow transport process, but must pay attention to the interaction between the precursor and the surface.

Recently, some experiments on the growth of amorphous films in LPCVD have demonstrated that the growth exponent β is substrate temperature dependent. Figure 1 summarizes some recent experimental results for amorphous silicon grown at different substrate temperatures [8–11]. The general trend is that β increases with decreasing substrate temperature and can span from 0.08 to 0.55. Similar temperature dependence was also observed in LPCVD of

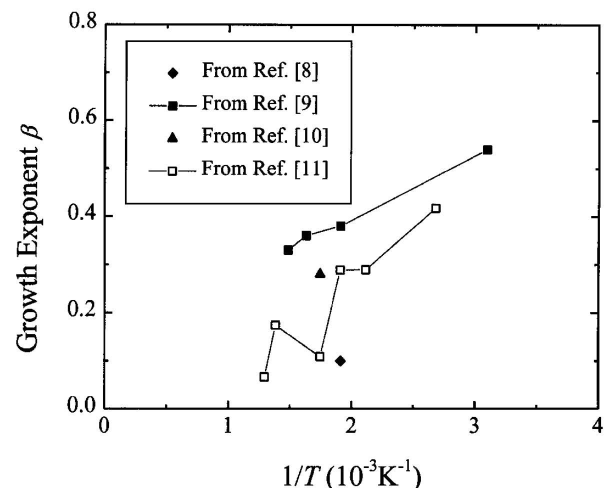

FIG. 1. The growth exponent β as a function of substrate temperature for various amorphous silicon CVD films found in the literature.

 © 2001 The American Physical Society

SiO_2 [5]. This kind of behavior cannot be explained in the usual framework of surface diffusion, condensation/evaporation, or KPZ growth. For example, for high temperature deposition, one might expect that surface diffusion of precursors plays a major role, so that the growth exponent should be close to 0.25 [2,3]. But this is not the case for the experiments shown in Fig. 1. In reality, in the LPCVD process, the precursors arrive at the substrate from all directions, and the shadowing effect plays an important role. The strength of the shadowing effect is closely related to the sticking coefficient of the precursor, which is the probability of the impinging flux reacting with the substrate. Changing the substrate temperature can alter the sticking coefficient of the precursor. For amorphous Si and LPCVD of SiO_2, the sticking coefficient decreases with increasing substrate temperature, which happens to match the trend in the change of the growth exponent β [12,13]. Thus, the substrate temperature changes the strength of the shadowing. Therefore, a growth model that explicitly includes the sticking coefficient is needed to explain the general trend of the growth behavior for different substrate temperatures.

If only the shadowing effect were present, one would expect $\beta = 1$, no matter how small the shadowing effect is [1]. Therefore, there must be mechanisms other than shadowing present. When a flux of the precursors is incident on the substrate, this flux either sticks to the surface at the point of incidence or is redistributed according to a certain reemission mode. This redistributed flux may reach another point of the surface and repeat the same process again. This kind of reemission process has been studied extensively for LPCVD via filling [14,15]. Recently, we have successfully applied the reemission model to interpret the unusual roughening behavior of plasma etch fronts [16], but so far this model has not been applied to growth front roughening. In the present work, we report the results on the effect of surface reemission on the morphology evolution of LPCVD growth fronts. We show that the surface morphology changes from a self-affine fractal to a columnarlike morphology with increasing sticking coefficient, which agrees qualitatively with experimental observations.

The roughening dynamics of reemission can be written as a nonlocal KPZ type equation [16]:

$$\frac{\partial h}{\partial t} = -\kappa\nabla^4 h + \sqrt{1 + (\nabla h)^2} \times [s_0 F_0(\boldsymbol{r}, t) + s_1 F_1(\boldsymbol{r}, t) + \ldots] + \eta \,, \tag{1}$$

where the term $-\kappa\nabla^4 h$ is caused by surface diffusion, and η is the noise. In this model, the probability of an incoming (zeroth-order) particle sticking to the surface is s_0, where s_0 is called the zeroth-order sticking coefficient. An nth-order particle that has been reemitted is called an $(n + 1)$th-order particle. The probability of an nth-order particle sticking is s_n. Detailed expressions for the overall flux $F_n(\boldsymbol{r}, t)$ of nth-order particles can be found in Ref. [16]. Clearly, zeroth-order reemission is just the shadowing effect. If all the s_n are equal and very small, the variation of the precursor concentration that would exist if only the shadowing term were present is balanced by higher-order reemission terms. In other words, if the flux redistribution is quick compared to the morphological evolution, the reemitted flux will reach all parts of the surface that were shadowed, giving a uniform concentration over it, satisfying that condition for KPZ growth implicitly. If the zeroth-order sticking coefficient is high, the shadowing effect will be present in Eq. (1), and the higher orders of reemission will no longer balance this effect. To demonstrate the effect of varying the zeroth-order sticking coefficient on surface morphology, we performed Monte Carlo simulations for first-order reemission for different values of the zeroth-order sticking coefficient by assuming thermal reemission. That is, s_1 is held equal to 1, while s_0 is varied. The details of the simulation are described in Ref. [17]. The surface is assumed to be described by a height function $h(x, y)$ defined on a periodic $N \times N$ lattice. The periodic boundary condition is applied. The simulation proceeds one particle at a time. First, a random position in the x-y plane is chosen for the particle. The initial position of the particle in the h direction is always one position higher than the maximum of the surface. Next, the direction that the particle will go off in is chosen; the distribution of directions depends on the properties of the incident flux. Specifically, we chose the distribution

$$\frac{dP}{d\Omega} = \frac{\cos\theta}{\pi} \,, \tag{2}$$

where the angle θ is measured with respect to the z axis. This distribution is based on the assumption that incident particles come from a gas containing particles traveling in all directions with equal probability. The particle moves in the chosen direction until hitting the surface, after which it can deposit on the surface or be reemitted according to the cosine distribution (thermal reemission). If it is reemitted, the particle will travel until it hits the surface again, or passes above the highest point on the surface. Once the particle has deposited on the surface or has passed above the highest point on the surface (meaning it will never hit the surface), the above procedure is repeated for a new particle. Also, to avoid overhangs, a particle that hits the side of a column will slide down the column before sticking on the surface. Figure 2 shows the surface morphology for different sticking coefficients. For small s_0 (<0.4), the surface has a self-affine fractal structure, and one cannot observe any wavelength selection. For $s_0 > 0.5$, a grainlike structure gradually develops, and the boundary between different grains becomes more distinct with increasing s_0. Therefore the surface morphology experiences a transition as s_0 is increased.

The growth exponent β and roughness exponent α, extracted from $H(\mathbf{r}, t)$, for different zeroth-order sticking coefficients, are shown in Fig. 3. The growth exponent β

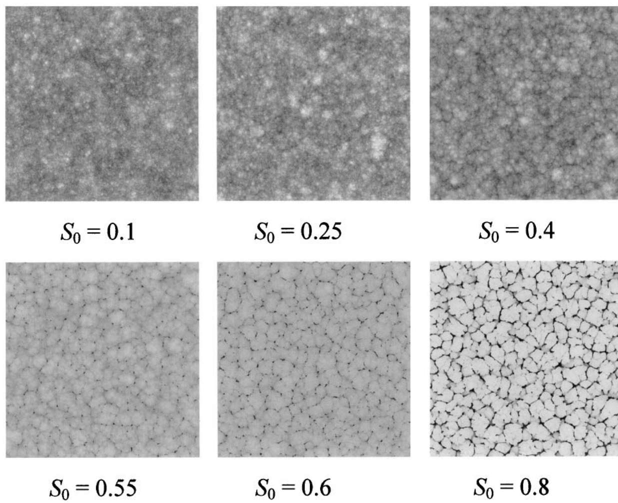

FIG. 2. The simulated growth morphology for different zeroth-order sticking coefficients for first-order reemission. The system size for each simulation is 1024 × 1024. The white in the grey scale means high, while black means low.

gradually increases with increasing s_0 (<0.5). This trend agrees qualitatively with the experimental results shown in Fig. 1. When s_0 increases from 0.5 to 0.7, β increases dramatically from 0.32 to 1.0. After β reaches 1.0, it stays the same for higher values of s_0. The roughness exponent α increases from 0 to 0.34 when s_0 changes from 0.05 to 0.5. For $s_0 > 0.5$, since the grain structure starts to appear, the surface morphology is not self-affine anymore, and there is no well defined α that can be extracted. One should notice that, when $s_0 \ll 1$, the reemission model gives $\beta = \alpha = 0$, as well as $z = 2$. These are exactly the exponents of the Edwards-Wilkinson (EW) growth model [2,3,18]. However, the reemission model is a nonlocal growth model (the growth rate at a certain point depends on the surrounding environment of the surface), while the EW model is a local growth model. (The surface relaxation rate at a certain point depends only on the curvature at that point.) Therefore, the reemission model and the EW model should belong to two different universality classes, yet they both give the same scaling exponents. Thus, the correspondence between universality classes and scaling exponents may not be one-to-one.

The first-order reemission model is the simplest case of our proposed growth model. Another extreme occurs when all sticking coefficients are the same (e.g., $s = s_0 = s_1 = s_2 = \ldots$). Figure 3 also shows β and α values, for different sticking coefficients, obtained from the Monte Carlo simulation for all-order reemission. For very small s ($= 0.05$), we obtain $\beta = 0.21$ and $\alpha = 0.28$. These values are not particularly close to the more accurate KPZ exponents, $\beta = 0.2445 \pm 0.0025$ and $\alpha = 0.393 \pm 0.003$ calculated numerically [19]. However, we have shown that as s approaches zero, the flux distribution near a surface will reach a constant value, and the growth mechanism will approach KPZ growth [20]. Hence, we would expect the exponents for all-order reemission to approach the KPZ exponents as s approaches zero. The fact that the small sticking coefficient exponents are not very close to the KPZ exponents is probably due to crossover effects, and we would expect larger (larger system size and longer time) simulations to yield better agreement with the KPZ equation. With increasing sticking coefficient, we again observe a transition of the morphology from self-affine to a grainlike structure.

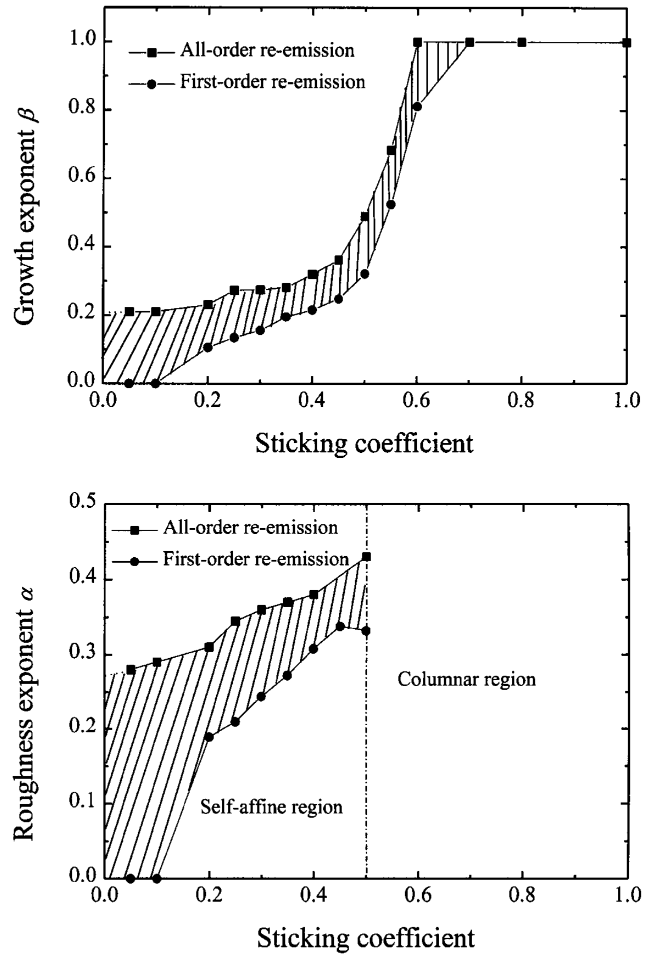

FIG. 3. The extracted growth exponent β and roughness exponent α from the height-height correlation function plotted as a function of sticking coefficient for first-order and all-order reemission. These two cases form the upper and lower extremes for finite-order reemission process. Exponents for finite-order reemission should fall in the shaded area.

In practice, precursors can lose energy during inelastic collisions with the substrate, and this can cause the sticking coefficient to vary for different orders of reemission. The results for different orders of reemission are shown in Table I and Fig. 4. In the inset of Fig. 4, we plot the results for zeroth-order reemission. One can see that, as the order of reemission increases, the growth exponent β increases. In fact, for small orders of reemission (≤ 4), the model gives a logarithmic dependence of interface width versus growth time (from which we could have concluded

TABLE I. The conditions for different orders of reemission.

Order of reemission	Sticking coefficient	Growth exponent β
1st	$s = s_0 = 0.05$ $s_1 = 1.0$	0.082
4th	$s = s_i = 0.05,\ i = 0,\ldots,3$ $s_4 = 1.0$	0.116
6th	$s = s_i = 0.05,\ i = 0,\ldots,5$ $s_6 = 1.0$	0.154
8th	$s = s_i = 0.05,\ i = 0,\ldots,7$ $s_8 = 1.0$	0.175
10th	$s = s_i = 0.05,\ i = 0,\ldots,9$ $s_{10} = 1.0$	0.178

that $\beta = 0$, as was done in Fig. 3 for first-order reemission with small sticking coefficient), while for higher orders of reemission, the growth exponent approaches the KPZ exponent. Therefore, first-order reemission and all-order reemission give the lower and upper bounds for the reemission model. The growth exponents and roughness exponents for finite-order reemission should fit within these bounds (i.e., in the shaded area in Fig. 3). For first-order reemission with small s_0, a valley receives more redistributed flux than a peak. Therefore, the valley has a higher growth rate than the peak, and the surface will be smooth. With the introduction of an additional order of reemission, the flux at the valley will have a greater probability to reemit from the surface. Therefore, compared to the first-order reemission, the growth rate at the valley for second-order reemission will be much lower, and the smoothening effect will be weaker. Thus, the growth exponent β will be larger. Clearly, different orders of reemission play different roles in the reemission model; i.e., they do not impose the exact same effect on the growth front. Therefore, the

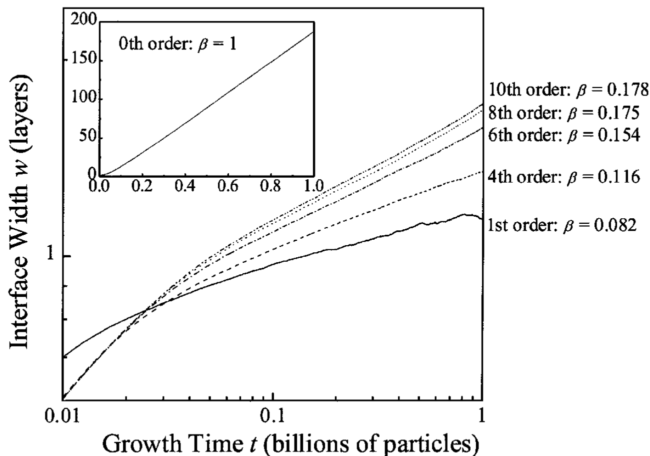

FIG. 4. The interface width w plotted as a function of the growth time t in log-log scale for different orders of reemission. The nth order reemission is defined as $s_n = 1$, and $s_i = 0.05$ for $i = 0$ to $n - 1$. The system size for the simulation is 1024×1024. The inset is a plot of w versus t for zeroth-order reemission in linear scale. The units for the inset are the same as for the main plot.

detailed balance of different orders of reemission will tune the observed growth dynamics.

In conclusion, we have studied, in detail, the effect of reemission on the morphology evolution during LPCVD. Using the reemission model, we have shown that the surface morphology changes from self-affine to a columnar-like morphology as the sticking coefficient is increased, which agrees qualitatively with experimental observations. Similar treatment may also be extended to sputter growth since LPCVD and sputter growth have many similar features.

This work was supported by NSF and MARCO Interconnect Focus Center.

[1] *Dynamics of Fractal Surfaces,* edited by F. Family and T. Viscek (World Scientific, Singapore, 1991).
[2] A.-L. Barabási and H.E. Stanley, *Fractal Concepts in Surface Growth* (Cambridge University Press, New York, 1995).
[3] P. Meakin, *Fractals, Scaling, and Growth Far from Equilibrium* (Cambridge University Press, Cambridge, 1998).
[4] M. Kardar, G. Parisi, and Y.-C. Zhang, Phys. Rev. Lett. **56**, 889 (1986).
[5] F. Ojeda, R. Cuerno, R. Salvarezza, and L. Vázquez, Phys. Rev. Lett. **84**, 3125 (2000).
[6] G.S. Bales, A.C. Redfield, and A. Zangwill, Phys. Rev. Lett. **62**, 776 (1989).
[7] C.-C. Hwang, H.-Y. Yang, J.-Y. Hsieh, and Y.-M. Dai, Thin Solid Films **304**, 371 (1997), and references therein.
[8] D.M. Tanenbaum, A.L. Laracuente, and A. Gallagher, Phys. Rev. B **56**, 4243 (1997).
[9] M. Kondo, T. Ohe, K. Saito, T. Nishimiya, and A. Matsuda, J. Non-Cryst. Solids **227–230**, Pt. II, 890 (1998).
[10] A.J. Flewitt, J. Robertson, and W.I. Milne, J. Appl. Phys. **85**, 8032 (1999).
[11] A. Smets, E. Kessels, B. Korevaar, C. Smit, R. van de Sanden, and D. Schram (unpublished).
[12] D.L. Smith, *Thin-Film Deposition—Principles and Practice* (McGraw-Hill, New York, 1995).
[13] M. Konuma, *Film Deposition by Plasma Techniques* (Springer-Verlag, Berlin, 1992).
[14] V.K. Singh, E.S.G. Shaqfeh, and J.P. McVittie, J. Vac. Sci. Technol. B **10**, 1091 (1992).
[15] For a review, see T.S. Cale and V. Mahadev, in *Thin Films—Modeling of Film Deposition for Microelectronic Applications,* edited by S. Rossnagel (Academic Press, San Diego, 1996), Vol. 22, p. 176.
[16] Y.-P. Zhao, J.T. Drotar, G.-C. Wang, and T.-M. Lu, Phys. Rev. Lett. **82**, 4882 (1999); J.T. Drotar, Y.-P. Zhao, T.-M. Lu, and G.-C. Wang, Phys. Rev. B **61**, 3012 (2000).
[17] J.T. Drotar, Y.-P. Zhao, T.-M. Lu, and G.-C. Wang, Phys. Rev. B **62**, 2118 (2000).
[18] S.F. Edwards and D.R. Wilkinson, Proc. R. Soc. London A **381**, 17 (1982).
[19] E. Marinari, A. Pagnani, and G. Parisi, J. Phys. A **33**, 8181 (2000).
[20] J.T. Drotar, Y.-P. Zhao, T.-M. Lu, and G.-C. Wang, Mater. Res. Soc. Symp. Proc. **648**, 7.9 (2001).